

Ultra-narrow-linewidth, single-frequency distributed feedback waveguide laser in $\text{Al}_2\text{O}_3:\text{Er}^{3+}$ on silicon

E. H. Bernhardt,^{1,*} H. A.G.M. van Wolferen,² L. Agazzi,¹ M. R.H. Khan,³ C. G.H. Roeloffzen,³
K. Wörhoff,¹ M. Pollnau,¹ and R. M. de Ridder¹

¹*Integrated Optical MicroSystems Group, MESA+ Institute for Nanotechnology, University of Twente, P.O. Box 217, 7500 AE Enschede, The Netherlands*

²*Transducers Science and Technology Group, MESA+ Institute for Nanotechnology, University of Twente, P.O. Box 217, 7500 AE Enschede, The Netherlands*

³*Telecommunication Engineering Group, Faculty of Electrical Engineering, Mathematics and Computer Science, University of Twente, P.O. Box 217, 7500 AE Enschede, The Netherlands*

*Corresponding author: E.H.Bernhardt@ewi.utwente.nl

Received March 30, 2010; revised June 21, 2010; accepted June 23, 2010;
posted June 28, 2010 (Doc. ID 126222); published July 8, 2010

We report the realization and performance of a distributed feedback channel waveguide laser in erbium-doped aluminum oxide on a standard thermally oxidized silicon substrate. The diode-pumped continuous-wave laser demonstrated a threshold of 2.2 mW absorbed pump power and a maximum output power of more than 3 mW with a slope efficiency of 41.3% versus absorbed pump power. Single-longitudinal-mode and single-polarization operation was achieved with an emission linewidth of 1.70 ± 0.58 kHz (corresponding to a Q factor of 1.14×10^{11}), which was centered at a wavelength of 1545.2 nm. © 2010 Optical Society of America

OCIS codes: 130.0130, 140.3570, 140.3490, 140.3500.

The ever-increasing demand for data bandwidth capacity in telecommunication networks necessitated the implementation of dense wavelength division multiplexing (DWDM). Because of their high-quality emission properties and broad wavelength tunability within the telecommunication C band (1525–1565 nm), single-frequency erbium-doped dielectric waveguide lasers offer a capable and competitive alternative to semiconductor distributed feedback (DFB) lasers for use in future DWDM networks [1].

Monolithic, single-frequency, dielectric lasers have been demonstrated in the form of DFB and distributed-Bragg-reflector cavities in a variety of erbium-doped dielectric materials, including silica [2], lithium niobate [3], as well as ion-exchanged [4] and femtosecond-laser-written [5] phosphate glass waveguides. Erbium-doped aluminum oxide ($\text{Al}_2\text{O}_3:\text{Er}^{3+}$) as a gain medium offers several advantages compared to these materials. It has a larger emission bandwidth than silica, which provides greater potential for wavelength tunability [6]. The relatively high refractive index of 1.65 and, hence, high refractive-index contrast between waveguide and cladding allow for the fabrication of more compact integrated optical structures and smaller waveguide cross sections. $\text{Al}_2\text{O}_3:\text{Er}^{3+}$ can be deposited on a number of substrates, including thermally oxidized silicon. This opportunity allows for integration with existing silicon-on-insulator waveguide technology. Recently, $\text{Al}_2\text{O}_3:\text{Er}^{3+}$ waveguides have been demonstrated with low background losses and an internal net gain over a wavelength range of 80 nm (1500–1580 nm), with a peak gain of 2.0 dB/cm at 1533 nm [7] and an $\text{Al}_2\text{O}_3:\text{Er}^{3+}$ integrated laser in a ring resonator geometry [8] has been shown to operate on several wavelengths in the range 1530–1557 nm.

In this Letter, we report a monolithic single-frequency DFB channel waveguide laser in $\text{Al}_2\text{O}_3:\text{Er}^{3+}$. The laser

output power surpasses that of the previously demonstrated ring laser by more than two orders of magnitude, while also providing the additional feature of single-polarization, single-longitudinal-mode emission with a linewidth as low as 1.70 ± 0.58 kHz.

The 1 μm thick channel waveguides were fabricated in an $\text{Al}_2\text{O}_3:\text{Er}^{3+}$ layer with an erbium concentration of $3 \times 10^{20} \text{ cm}^{-3}$, which was deposited onto an 8 μm thick thermally oxidized, 10 cm diameter standard silicon wafer by means of reactive cosputtering [9]. The ridge waveguides were 1 cm long, 3 μm wide, and were etched 0.1 μm deep via standard lithography and a reactive ion etching process [10]. A 650 nm thick SiO_2 cladding layer was deposited on top of the ridge waveguides by use of plasma-enhanced chemical vapor deposition. This waveguide geometry was designed to support only single transverse-mode operation at the 1480 nm pump and 1545.2 nm laser wavelengths for both TE and TM-polarized modes. The end facets of the optical chip were prepared by dicing.

Optical feedback in the cavity was provided by a surface-relief Bragg grating, which extended over the entire 1 cm length of the cavity. The grating pattern was defined in a 120 nm thick negative resist layer on top of the SiO_2 cladding by means of laser interference lithography. Finally, the grating pattern was etched into the SiO_2 layer by use of a $\text{CHF}_3:\text{O}_2$ reactive ion plasma, after which the residual resist was removed by an O_2 plasma. The resultant Bragg grating had an etch depth of ~ 150 nm with a period of 488 nm and a duty cycle of $\sim 50\%$. Figure 1 shows a top-view scanning electron microscope (SEM) image of the realized Bragg grating. To ensure single-longitudinal-mode laser operation, a quarter-wave phase shift was introduced to the DFB cavity. The phase shift was implemented by means of a 2 mm long adiabatic sinusoidal tapering of the waveguide width in the center region of the cavity [11,12]. Inside the phase-shift region, the waveguide width

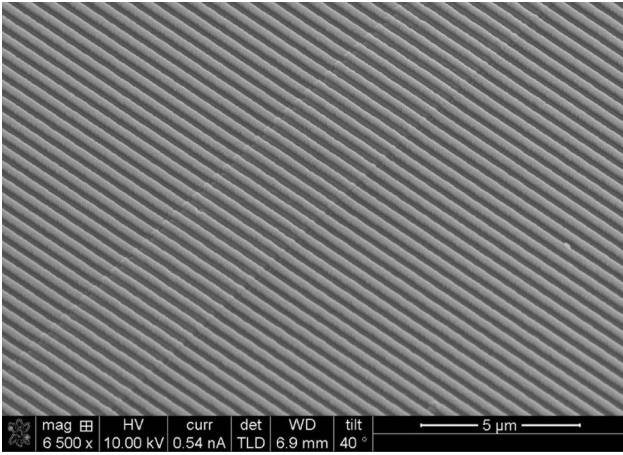


Fig. 1. Top-view SEM image of the Bragg grating. The $3\ \mu\text{m}$ wide ridge feature is due to the waveguide below the grating.

was increased adiabatically from $3.0\ \mu\text{m}$ to a maximum of $3.45\ \mu\text{m}$. By placing the phase shift asymmetrically with respect to the center of the cavity, a higher degree of laser outcoupling can be attained in the direction of the shorter end of the cavity. To optimize the laser output power, the phase shift was displaced $1\ \text{mm}$ from the center of the cavity. Consequently, by pumping the cavity from the end-facet nearer to the phase shift, the majority of the laser power was emitted in the direction of the pumped facet where the gain is highest. To manufacture the phase shift in this manner does not require any additional fabrication steps because the phase shift is defined during the same photolithographic step in which the waveguides are defined.

In the experimental setup shown in Fig. 2(a), the $\text{Al}_2\text{O}_3:\text{Er}^{3+}$ DFB laser was pumped by a $1480\ \text{nm}$ laser diode through a $1480/1550\ \text{nm}$ wavelength division multiplexer (WDM) fiber. The laser emission was collected from the pumped side of the cavity via the $1550\ \text{nm}$ port of the WDM, which was connected to a powermeter. The input port of a second $1480/1550\ \text{nm}$ WDM fiber was connected to the unpumped side of the cavity. Its $1480\ \text{nm}$ port was connected to a second powermeter to measure the unabsorbed pump power, while the $1550\ \text{nm}$ port was connected to an optical spectrum analyzer (OSA), with a maximum resolution of $0.1\ \text{nm}$, to determine the laser wavelength and to confirm single-longitudinal-mode behavior. Both WDM fibers were butt coupled to the respective ends of the optical chip by use of index-matching fluid at the fiber-chip interfaces. From insertion loss measurements, a fiber-chip coupling efficiency of 27% was determined for pump and laser wavelengths, as no fiber-chip coupling optimization was performed for this particular device. The maximum pump power that could be launched into the waveguide with this configuration was $67\ \text{mW}$. From mode overlap calculations, it is estimated that the fiber-chip coupling can be improved to $>90\%$ with an appropriate horizontal and vertical taper of the waveguide.

A slope efficiency of 41.3% versus absorbed pump power was achieved with a maximum laser output power of more than $3\ \text{mW}$ for an absorbed pump power of $10\ \text{mW}$; see Fig. 2(b). Further power scaling was limited by the available pump power. The laser threshold oc-

curred at $2.2\ \text{mW}$ of absorbed pump power. This low threshold is a consequence of the strong light confinement due to the relatively high refractive index of Al_2O_3 , which allows for the fabrication of small waveguide cross sections. The threshold and slope efficiency versus launched pump power are $15\ \text{mW}$ and 6.2% , respectively.

The laser operated at a wavelength of $1545.2\ \text{nm}$ and the emission was TE polarized. Because characterization of the Bragg gratings showed that the Bragg reflection of the TM mode occurs at $\sim 1533\ \text{nm}$, we conclude that the laser was operating TE polarized at all times. Although single-mode behavior could be confirmed with the OSA measurement, the linewidth of laser emission was limited by the $0.1\ \text{nm}$ resolution. Consequently, a delayed self-heterodyne interferometer [13] was implemented to measure the laser linewidth. The setup was constructed with two $50/50$ couplers, an $8.9\ \text{km}$ fiber, an $80\ \text{MHz}$ acousto-optic modulator, a photodetector, and an RF

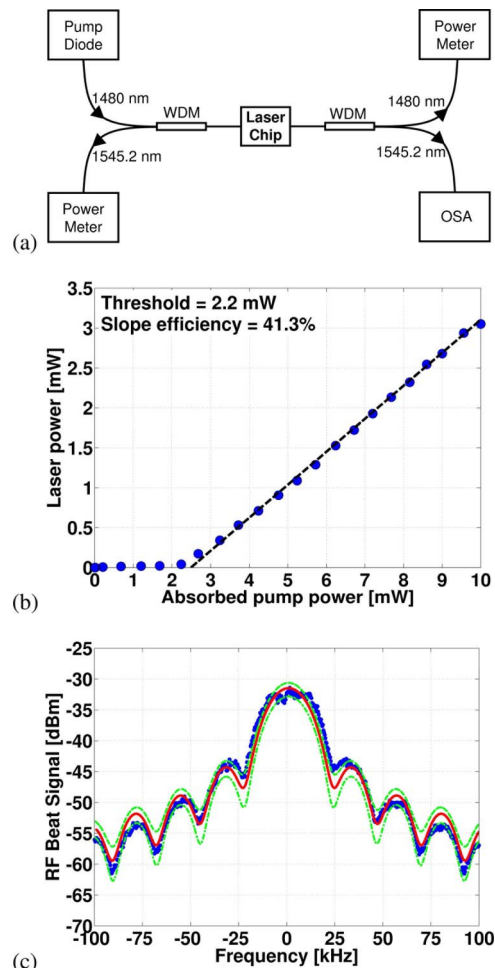


Fig. 2. (Color online) (a) Experimental setup used to characterize the DFB laser. (b) Laser output power of the DFB laser as a function of absorbed pump power (circles). The dashed line represents a linear fit with a slope efficiency of 41.3% . (c) Measured RF beat signal (circles), along with the best fitted theoretical RF power spectrum of a $1.70\ \text{kHz}$ Lorentzian linewidth (solid curve). The calculated RF power spectrum curves for Lorentzian linewidths of $1.70 + 0.58\ \text{kHz}$ (dashed curve) and $1.70 - 0.58\ \text{kHz}$ (dashed-dotted curve) enclose 68% of the measured data.

spectrum analyzer. The measured RF beat signal is shown in Fig. 2(c). The interference fringes that are observed in the measured RF power spectrum indicate that the coherence length of the DFB laser is considerably longer than the 8.9 km fiber, so that the two optical signals in the respective branches of the interferometer are still highly correlated. The Lorentzian laser linewidth cannot simply be inferred from this measurement because the Lorentzian line shape is distorted by the superimposed interference lobes. Instead, the laser linewidth for such a subcoherence delay length was extracted by a least-squares fit of the theoretical RF power spectrum to the measurement [14]. Initial measurements revealed a linewidth of 15 kHz, which was limited by mechanical vibrations in the measurement setup. By mounting the fiber-chip-coupling setup on an air-cushioned platform, the measured linewidth was reduced to a -3 dB Lorentzian laser linewidth of 1.70 kHz [see Fig. 2(c)], which corresponds to a coherence length of more than 55 km and a Q factor of 1.14×10^{11} . This linewidth is 0.9 kHz wider than the fundamental Schawlow-Townes limit of 0.8 kHz for this laser. To determine the uncertainty $\delta\nu$ in the laser linewidth, we calculated theoretical RF power spectra corresponding to Lorentzian linewidths of $1.70 \pm \delta\nu$ kHz, such that they enclose 68% (in analogy to one standard deviation) of the measured data. This method suggests a linewidth uncertainty of $\delta\nu = 0.58$ kHz. The calculated RF power spectra associated with Lorentzian linewidths of $1.70 + 0.58$ kHz and $1.70 - 0.58$ kHz are shown in Fig. 2(c). The linewidth is narrower than the 2.7 kHz linewidth produced by a discrete-mode laser diode, which was claimed to have been the narrowest linewidth of any free-running monolithic laser [15]. Standard semiconductor DFB lasers typically have linewidths that are a few orders of magnitude larger owing to longitudinal spatial hole burning when carriers are depleted by the nonuniform photon distribution [16]. This induces a refractive-index change, which results in a decreased grating reflectivity and, consequently, linewidth broadening.

In conclusion, we have demonstrated an $\text{Al}_2\text{O}_3:\text{Er}^{3+}$ monolithic DFB waveguide laser which, to the best of our knowledge, represents the first rare-earth-ion-doped DFB laser on a silicon substrate. This result holds many promising opportunities for the integration of such single-frequency lasers with existing waveguide technology on silicon substrates. The low-threshold laser demonstrated single-longitudinal-mode, single-polarization emission with a linewidth of 1.70 ± 0.58 kHz. A maxi-

mum output power of more than 3 mW was achieved with a slope efficiency of 41.3%. The broad emission spectrum of $\text{Al}_2\text{O}_3:\text{Er}^{3+}$ and the wafer-scale deposition process hold great potential for the realization of integrated DFB laser arrays that operate on the International Telecommunication Union Grid throughout the entire telecommunication C band.

The authors thank Meindert Dijkstra for assisting with the fabrication of the samples. This work was supported by funding through the Smartmix "Memphis" programme of the Dutch Ministry of Economic Affairs.

References

1. D. L. Veasey, D. S. Funk, N. A. Sanford, and J. S. Hayden, *Appl. Phys. Lett.* **74**, 789 (1999).
2. T. Kitagawa, F. Bilodeau, B. Malo, S. Theriault, J. Albert, D. C. Jihson, K. O. Hill, K. Hattori, and Y. Hibino, *Electron. Lett.* **30**, 1311 (1994).
3. B. K. Das, H. Suche, and W. Sohler, *Appl. Phys. B* **73**, 439 (2001).
4. L. Bastard, S. Blaize, and J. E. Broquin, *Opt. Eng.* **42**, 2800 (2003).
5. G. D. Marshall, P. Dekker, M. Ams, J. A. Piper, and M. J. Withford, *Opt. Lett.* **33**, 956 (2008).
6. G. N. van den Hoven, E. Snoeks, A. Polman, J. W. M. van Uffelen, Y. S. Oei, and M. K. Smit, *Appl. Phys. Lett.* **62**, 3065 (1993).
7. J. D. B. Bradley, L. Agazzi, D. Geskus, F. Ay, K. Wörhoff, and M. Pollnau, *J. Opt. Soc. Am. B* **27**, 187 (2010).
8. J. D. B. Bradley, R. Stoffer, L. Agazzi, K. Wörhoff, and M. Pollnau, *Opt. Lett.* **35**, 73 (2010).
9. K. Wörhoff, J. D. B. Bradley, F. Ay, D. Geskus, T. P. Blauwendraat, and M. Pollnau, *IEEE J. Quantum Electron.* **45**, 454 (2009).
10. J. D. B. Bradley, F. Ay, K. Wörhoff, and M. Pollnau, *Appl. Phys. B* **89**, 311 (2007).
11. H. Soda, Y. Kotaki, H. Sudo, H. Ishikawa, S. Yamakoshi, and H. Imai, *IEEE J. Quantum Electron.* **23**, 804 (1987).
12. L. Bastard and J. Broquin, *Proc. SPIE* **5728**, 136 (2005).
13. T. Okoshi, K. Kikuchi, and A. Nakayama, *Electron. Lett.* **16**, 630 (1980).
14. L. E. Richter, H. I. Mandelberg, M. S. Kruger, and P. A. McGrath, *IEEE J. Quantum Electron.* **22**, 2070 (1986).
15. R. Phelan, B. Kelly, D. Jones, C. Herbert, J. O'Carroll, M. Rensing, B. Cai, A. Kaszubowska-Anandarajah, P. Perry, J. Stopford, P. Anandarajah, L. P. Barry, and J. O'Gorman, in *Optical Fiber Communication Conference and Exposition and The National Fiber Optic Engineers Conference*, OSA Technical Digest (CD) (Optical Society of America, 2008), paper OThK5.
16. T. Kunii and Y. Matsui, *Opt. Quantum Electron.* **24**, 719 (1992).